# Dynamic Solvation in Room-Temperature Ionic Liquids†

**P. K. Chowdhury, M. Halder, L. Sanders, T. Calhoun, J. L. Anderson, D. W. Armstrong, X. Song, and J. W. Petrich***

*Department of Chemistry, Iowa State University, Ames, Iowa 50011*

*Received: December 2, 2003; In Final Form: April 20, 2004*

The dynamic solvation of the fluorescent probe, coumarin 153, is measured in five room-temperature ionic liquids using different experimental techniques and methods of data analysis. With time-resolved stimulated-emission and time-correlated single-photon counting techniques, it is found that the solvation is comprised of an initial rapid component of ∼55 ps. In all the solvents, half or more of the solvation is completed within 100 ps. The remainder of the solvation occurs on a much longer time scale. The emission spectra of coumarin 153 are nearly superimposable at all temperatures in a given solvent unless they are obtained using the supercooled liquid, suggesting that the solvents have an essentially glassy nature. The physical origin of the two components is discussed in terms of the polarizability of the organic cation for the faster one and the relative diffusional motion of the cations and the anions for the slower one. A comparison of the solvation response functions obtained from single-wavelength and from spectral-reconstruction measurements is provided. Preliminary fluorescence-upconversion measurements are presented against which the appropriateness of the single-wavelength method for constructing solvation correlation functions and the use of stimulated-emission measurements is considered. These measurements are consistent with the trends mentioned above, but a comparison indicates that the presence of one or more excited states distorts the stimulated-emission kinetics such that they do not perfectly reproduce the spontaneous emission data. Fluorescence-upconversion results indicate an initial solvation component on the order of ∼7 ps.

## Introduction

Room-temperature ionic liquids (RTILs) are becoming an increasingly rich area of study.[1,2] They have been used as novel solvent systems for organic synthesis,[3−16] for liquid−liquid extraction,[17,18] in electrochemical studies,[19] and as ultralow volatility liquid matrixes for matrix-assisted laser desorption/ionization mass spectrometry.[20] RTILs have other properties that make their application in chemical systems attractive. Some are immiscible with water and nonpolar organic solvents. They are stable to temperatures in excess of 300 °C, but they have negligible vapor pressures, thus making them "green" solvents by reducing environmental levels of volatile organic carbons. Their viscosities can easily be varied by changing their cationic or anionic constituents.

Most ionic liquids are said to have similar polarities, close to those of short-chain alcohols.[21−24] The solvatochromic effect of Reichardt's dye[21] and Nile Red[22] as well as of fluorescent probes[23,24] and the Rohrschneider−McReynolds gas−liquid chromatography (GLC) method[25] have been used to characterize ionic liquids by obtaining a general, one-dimensional polarity-based parameter. This approach has not been successful for RTILs because they all fall within the same narrow range of values.[21−24] Yet, two different ionic liquids that have essentially identical "polarity," as measured by such methods, can produce very different results when used as solvents for organic reactions, GLC, or extractions. Most recently, we have used the solvation parameter model developed by Abraham, which has been developed to characterize either liquid- or gas-phase interactions between solute molecules and liquid phases.[26−28] This model is based on a linear free-energy relationship. The solute retention factor is determined chromatographically for a set of probe solutes, and a multiple linear regression analysis relates it to a set of five parameters that characterize the solvent.[2]

Solvent properties can dramatically influence the rate of chemical reactions. Assuming equilibrium solvation along the reaction coordinate, many of these effects can indeed be explained by classical thermodynamics, as the construction of the above linear free-energy relationships attempts. A thermodynamic approach is valid, however, only if the motion of the solvent molecules is very fast compared with the motion along the reaction coordinate, so that the solvent is always in equilibrium with the solute. In particular, the solvent relaxation time scales influence the dynamics of electron transfer, proton transfer, and other charge-transfer reactions by exerting a time-dependent dielectric friction. In these cases, reaction rates may be limited by the rate of solvent relaxation.[29,30] A well-established method to measure time-dependent solvation is by means of time-resolved fluorescence spectroscopy. After short-pulse excitation, the fluorescence spectrum of a probe solute red shifts in time as the surrounding solvent re-equilibrates to the new, excited-state charge distribution. This time-dependent fluorescence shift provides a direct measure of the kinetics of solvation occurring at the microscopic level relevant to chemical reactions.[29]

Before the availability of RTILs, transient solvation by ions was studied by Huppert and co-workers using molten salts[31,32] and by Maroncelli and co-workers using nonaqueous solutions of dissolved ions.[33] The dynamic aspects of solvation by RTILs are becoming an object of experimental and theoretical studies. The dynamic solvation and the reorientational behavior of several probe molecules in different ionic liquids have recently

† Part of the special issue "Gerald Small Festschrift".

* To whom correspondence may be addressed. E-mail: jwp@iastate.edu.

10.1021/jp0376828 CCC: $27.50 
Published on Web 06/02/2004

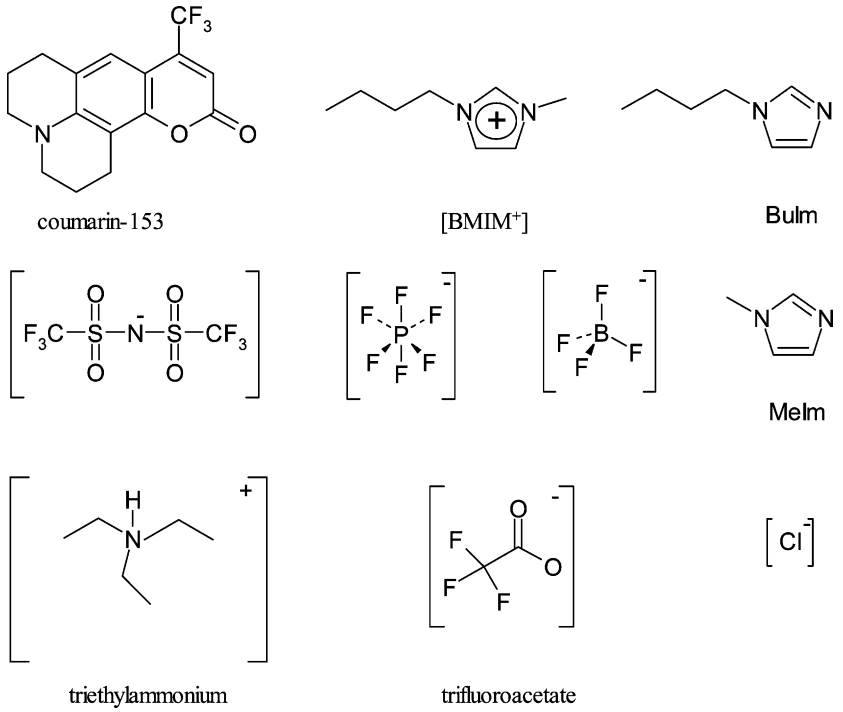


**Figure 1.** The solvation probe, coumarin 153, and 4 RTILs, ([BMIM$^+$][Cl$^-$], [BMIM$^+$][$BF_4^-$], [BMIM$^+$][$PF_6^-$], and [BMIM$^+$][$NTf_2^-$]), formed from the 1-butyl-3-methylimidazolium cation and the four anions indicated ([$NTf_2^-$] is $(CF_3SO_2)_2N^-$); one RTIL formed from the triethylammonium cation and trifluoroacetate ([$NHEt_3^+$][$TFA^-$]); butylimidazole and methylimidazole.

been investigated.[34−39] These workers have shown that the solvation dynamics is biphasic. A molecular dynamics simulation by Shim et al.[40] has been interpreted in terms of the faster component corresponding to diffusional motion of the anion and the slower component corresponding to collective motion of the anion and the cation. In addition, Hyun et al.[41] and Giraud et al.[42] have used the optical Kerr effect to study the low-frequency vibrational motions ($<200$ cm$^{-1}$) of these solvents.

In this article, we address the dynamic aspects of solvation by RTILs using Stokes shift data of the fluorescent probe, coumarin 153 (Figure 1), from the sub-picosecond to the nanosecond time regimes. We investigate four RTILs based on the 1-butyl-3-methylimidazolium cation, BMIM$^+$, and either the $Cl^-$, $BF_4^-$, $PF_6^-$, or $(CF_3SO_2)_2N^-$ anions (Figure 1). They are typically referred to as [BMIM$^+$][$Cl^-$], [BMIM$^+$][$BF_4^-$], [BMIM$^+$][$PF_6^-$], and [BMIM$^+$][$NTf_2^-$], respectively. We compare these RTILs with the organic subunits, butylimidazole and methylimidazole. A fifth ionic liquid studied is [$NHEt_3^+$][$TFA^-$], triethylammonium trifluoroacetate. Major conclusions are that the rapid initial phase of solvation arises from the cation and that the simulations of Shim et al.[40] may not provide an appropriate comparison for large organic fluorescent solvation probes, such as coumarin 153. In the course of this work, comparisons were made between different methods of constructing the solvation correlation function and of obtaining the solvation data itself. Consequently, this work addresses aspects of methodology nearly as much as the problem of solvation by RTILs.

The plan of the article is as follows. After a description of the various experimental and data-treatment methods, we present the results. It became apparent during the course of the investigation that they depend sometimes rather significantly on the type of experiment or data treatment used. The discussion section is separated into three parts. The first is a short consideration of the steady-state spectra of the RTILs. The second deals with the early stages of this work, where the long-time behavior (up to 4 ns) of RTILs was studied by time-correlated single-photon counting and the early events by transient absorption (stimulated emission), the latter of which employed a particular method of constructing the solvation correlation function using a single probe wavelength. Although these methods produced results obeying reasonable trends, it became apparent that neither measurement of stimulated-emission nor single-wavelength analysis was adequate. The third part of the discussion provides a comparison with results from upconversion measurements that offer a more traditional and direct measure of spontaneous emission. Salient points are summarized in the conclusions section.

## Materials and Methods

**RTILs.** 1-Butyl-3-methylimidazolium chloride [BMIM$^+$][$Cl^-$] is produced by refluxing equimolar amounts of 1-methylimidazole with 1-chlorobutane at 70 °C for 72 h. The resulting [BMIM$^+$][$Cl^-$] is washed with ethyl acetate and dried under vacuum. 1-Butyl-3-methylimidazolium tetrafluoroborate [BMIM$^+$][$BF_4^-$] is produced by mixing 10 g of [BMIM$^+$][$Cl^-$] (0.057 mol) in ∼100 mL of acetone. Sodium tetrafluoroborate (6.29 g (0.057 mol)) is added and stirred for 24 h. The resulting sodium chloride is filtered off and the acetone removed under vacuum. 1-Butyl-3-methylimidazolium hexafluorophosphate [BMIM$^+$][$PF_6^-$] is produced by dissolving 164.49 g (0.94 mol) of [BMIM$^+$][$Cl^-$] in ∼250 mL of water and reacting an equimolar amount (0.94 mol) of hexafluorophosphoric acid ($HPF_6$) and stirring for 24 h. The resulting [BMIM$^+$][$PF_6^-$] is washed with water until the washings are no longer acidic. The IL is then dried under vacuum. Hexafluorophosphoric acid is corrosive, toxic, and should be handled with care. 1-Butyl-3-methylimidazolium bis[(trifluoromethyl)-sulfonyl]imide, [BMIM$^+$][$NTf_2^-$], is produced by dissolving 34.0 g (0.118 mol) of *N*-lithiotrifluoromethanesulfonimide in ∼150 mL of water and mixing with 20.67 g (0.118 mol) of [BMIM$^+$][$Cl^-$] also dissolved in ∼150 mL water. The mixture is stirred for 12 h. The aqueous portion is removed and the resulting ionic liquid

washed with water and then dried under vacuum. All RTILs produced using the $[BMIM^+][Cl^-]$ salt are subjected to the silver nitrate test to ensure no chloride impurities remain in the samples. $[NHEt_3^+][TFA^-]$ is prepared by adding a slight molar excess of trifluoroacetic acid dropwise to triethylamine in a 50-mL round-bottom flask. The mixture is then heated at 40 °C and stirred for 2 h. Excess trifluoroacetic acid is removed under vacuum and the remaining ionic liquid dried through a silica gel column and stored under $P_2O_5$.

**Spectroscopic Measurements and Data Analysis.** Butylimidazole (>98% purity) and methylimidazole (>99% purity) were obtained from Aldrich (St. Louis, MO) and dried over molecular sieves (type 4A) before use. During spectroscopic measurements, the quartz cuvettes were kept tightly sealed so as to prevent moisture from being absorbed by the ionic liquids. The temperature-dependent measurements were carried out in a thermoelectric temperature-controlled cuvette holder (Quantum Northwest, WA), permitting regulation over the range −40 to 100 °C. All ionic liquids were carefully dried before optical measurements were performed. Silica gel of 60−200 mesh is activated at 150 °C. A small silica gel column is prepared using a Pasteur pipet, and the pure ionic liquid is added to the column. Depending on the viscosity of the ionic liquid, a bulb is used to force the ionic liquid through the silica gel column. Once the ionic liquid emerges from the column, it is stored in a desiccator under $P_2O_5$ until further use. The RTILs were subsequently dried over molecular sieves: Type 4A, GRADE 514, 8-12 Mesh, and with effective pore size of 4 Å.

**Steady-State Measurements.** Steady-state excitation and emission spectra were recorded with a SPEX Fluoromax with a 4-nm band pass and were corrected for detector response. A 1-cm path length quartz cuvette was used for the measurements. The steady-state spectra can be used to compute the reorganization energy, $\lambda$, by means of[43]

$$\lambda = \hbar \frac{\int_0^\infty d\upsilon[\sigma_a(\upsilon) - \sigma_f(\upsilon)]\upsilon}{\int_0^\infty d\upsilon[\sigma_a(\upsilon) + \sigma_f(\upsilon)]} \quad (1)$$

The $\sigma_{a,f}$ are the absorption (or excitation) and emission spectra, respectively, on a wavenumber scale. The reorganization energy is widely used as a measure of the strength of interactions between a chromophore and its surrounding dielectric media in solvation dynamics studies. It is usually taken as half of the Stokes shift. This estimation is accurate if the excitation and emission spectra are Gaussian, but it becomes unreliable if they are not. The actual computation of $\lambda$ is accomplished by first manipulating the emission and excitation spectra to permit their addition and subtraction. This requires normalized spectra consisting of equally spaced points. We interpolate and renormalize them so as to obtain spectra having 20-$cm^{-1}$ spacing between each point and then shift the crossing point of the two curves so that it lies at 0 $cm^{-1}$. The spectral baselines are then corrected by subtracting the lowest intensity and renormalizing. This manipulation is motivated by the low-intensity emission near 800 nm and questions concerning the utility of the correction factors of our fluorimeter in this region. In any case, baseline subtraction is minor and changes the final result by approximately 1%. An appropriate number of zeros is added to the high-energy end of the emission spectrum and to the low-energy end of the excitation spectrum so that the curves can be added and subtracted along their entire breadths. $\lambda$ may now be calculated according to eq 1. In practice, however, the integration is more conveniently performed from negative infinity to zero instead of from zero to positive infinity to avoid interference from transitions to higher-lying excited states. Taking these limits of integration is permitted as long as there is mirror image symmetry between the emission and excitation spectra. Time-resolved spectra are treated similarly, but the emission data first must be continued down to zero intensity, since it is impractical to obtain time-resolved and spectrally resolved data out into the wings of the emission spectrum. This continuation is done simply by connecting the last two points of the available data with straight lines that extend to zero. These new curves consisting of the data points and the straight lines are interpolated in the same way as the steady-state excitation curve. The value of $\lambda$ is sensitive to the way in which the spectrum is continued. We have used both straight-line and log-normal continuations but have opted for the simplest. The errors introduced in the continuation are effectively canceled when time-dependent $\lambda$s are compared with each other (as opposed to the steady-state spectrum) as they are in Table 1, which furnishes $\lambda$ at 100 and 4000 ps. The rest of the process proceeds as above. All data manipulations were performed with Microcal Origin 7.0.

**Time-Resolved Measurements.** The laser source for the time-correlated single-photon counting measurements was a homemade mode-locked Ti−sapphire laser, tunable from 780 to 900 nm with a repetition rate of 82 MHz. The fundamental from the Ti−sapphire oscillator was modulated by a Pockels cell (Model 350-160, Conoptics Inc) to reduce the repetition rate to about 8.8 MHz and was subsequently frequency doubled by focusing tightly into a 0.4-mm BBO crystal. The resulting blue light, which had a central wavelength of 425 nm, provided the excitation source. The fluorescence decays were collected at the magic angle (polarization of 54.7° with respect to the vertical). Emission was collected through a single monochromator (ISA H10) fitted with a slit having an 8-nm band pass. A half-wave plate before a vertical polarizer ensured the polarization of the excitation light. The instrument-response function of the apparatus had a full-width-at-half-maximum (fwhm) of 80 ps. A cuvette of 1-cm path length was used for the time-resolved measurements of C153 in the different solvents. To construct the time-resolved spectra, a series of decays (~3000 counts in the peak channel) were collected over as much of the fluorescence spectrum as possible and were fit to a maximum of three exponentials, yielding fits with $\chi$-squared values of ~1. Transient spectra were reconstructed from these fits by normalizing to the steady-state spectra of the samples according to the equation[29]

$$S(\lambda,t) = D(\lambda,t) \frac{S_0(\lambda)}{\int_0^\infty D(\lambda,t)\, dt} \quad (2)$$

$D(\lambda,t)$ is the wavelength-resolved fluorescence decay; $S_0(\lambda)$ is the steady-state emission intensity at a given wavelength. We have employed the traditional approach of fitting the time-resolved spectra to a log-normal line-shape function, from which we extract the peak frequency, $\nu(t)$, as a function of time. The solvation dynamics were described by the normalized correlation function as follows[29]

$$C(t) = \frac{\nu(t) - \nu(\infty)}{\nu(0) - \nu(\infty)} \quad (3)$$

$\nu(0)$ is the frequency at zero time, that is, immediately after excitation. $\nu(\infty)$ is the frequency at "infinite time," the maximum of the steady state fluorescence spectrum. The decays used to

**TABLE 1: Spectral Characteristics of Coumarin 153 in Some RTILs**

| ionic liquid[a] | melting point[b] (°C) | $\eta$ (cP) | $\langle\nu\rangle_{abs}$[d] ($cm^{-1}$) | $\langle\nu\rangle_{em}$[d] ($cm^{-1}$) | $\lambda$[e] ($cm^{-1}$) | $\lambda_{100ps}$[f,g] ($cm^{-1}$) | $\lambda_{4000ps}$[f,g] ($cm^{-1}$) | $\langle\tau\rangle_{SR}$[h] (ns) | $\langle\tau\rangle_{SW}$[i] (ns) |
|---|---|---|---|---|---|---|---|---|---|
| $[BMIM^+][Cl^-]$ (30 °C) | 65 | 11000[c] | 23490 | 18570 | 2294 | 1940 | 2112 | 2.0 | 1.7 |
| $[BMIM^+][Cl^-]$ (70 °C) | 65 | 334[c] | 23540 | 18090 | 2582 | 2285 | 2627 | 0.53 | 0.33 |
| $[BMIM^+][PF_6^-]$ (20 °C) | −8 | 371[c] | 24080 | 18420 | 2592 | 2015 | 2313 | 1.0 | 0.38 |
| | | 312[b] | $1.4 \pm 0.3$[j] | | | | | | |
| | | $1.8 \pm 0.4$[k] | | | | | | | |
| | | $3.35 \pm 0.02$[l] | | | | | | | |
| | | $6.47 \pm 0.20$[s] | | | | | | | |
| $[BMIM^+][BF_4^-]$ (20 °C) | −82 | 154[c] | 23670 | 18350 | 2481 | 1968 | 2203 | 0.46 | 0.31 |
| | | 233[b] | 1.44[m] | | | | | | |
| | | 2.13[n] | | | | | | | |
| $[BMIM^+][NTf_2^-]$ (20 °C) | −4 | 52[b] | 24110 | 18530 | 2607 | 1965 | 2180 | 0.72 | 0.17 |
| | | $0.28 \pm 0.04$[o] | | | | | | | |
| | | $0.48 \pm 0.07$[p] | | | | | | | |
| | | $0.56 \pm 0.08$[q] | | | | | | | |
| | | $0.38 \pm 0.06$[r] | | | | | | | |
| butylimidazole (20 °C) | | < 50 | 24040 | 18700 | 2622 | 2263 | 2344 | 0.070 | 0.041 |
| methylimidazole (20 °C) | | < 50 | 24000 | 18330 | 2672 | 2484 | 2480 | 0.050 | 0.025 |
| $[NHEt_3^+][TFA^-]$ (20 °C) | | 26100 | 19450 | 2836 | 2451 | 2764 | 0.42 | 0.27 | |

[a] For abbreviations, see the caption to Figure 1. Although the melting point of $[BMIM^+][Cl^-]$ is ~65 °C,[57] it usually takes several days at room temperature before it solidifies. [b] From ref 57. [c] From ref 52. [d] $\langle\nu\rangle = (\int_0^\infty \nu I(\nu)\, d\nu / \int_0^\infty I(\nu)\, d\nu)$, computed using 70% of the emission and excitation spectra in order to exclude the contributions from absorption to states higher than $S_1$ in energy. [e] Computed from eq 1. See text and ref 43. [f] The reorganization energies at 100 and 4000 ps are computed as discussed in the Experimental Section. Note that, because of the limited data set used to obtain the time-resolved spectra, the $\lambda$ at 4000 ps deviate from the steady-state values, for which in most cases we would expect them to be approximately the same. [g] The fractional amount of solvation at 100 ps, for example, can be determined by $f_{100ps} = (\lambda_{100ps} - \lambda_i/\lambda_{4000ps} - \lambda_i)$, where $\lambda_i$ is the intramolecular contribution to the reorganization energy. Maroncelli and co-workers have addressed the estimation of $\lambda_i$ by proposing methods to compute the "zero-time" spectrum arising only from solvation.[58] [h] Average solvation times obtained from the spectral-reconstruction data, computed from the fit parameters given in the caption to Figure 4. The comparison of the average solvation times is made using only data accumulated from time-correlated single-photon counting data. Errors in the solvation times are ~±15%. [i] Average solvation times obtained from the single-wavelength data. The average time is computed from the spliced picosecond and nanosecond experiments. [j] At 25 °C using 4-aminophthalimide (4-AP).[37] [k] At 25 °C using coumarin 102.[37] [l] At 25 °C using coumarin 153.[38] [m] At 20 °C using 6-propionyl-2-dimethylaminonaphthalene (Prodan).[35] [n] At room temperature using coumarin 153.[34] [o] At 25 °C using coumarin 153. The average solvation time is computed from parameters obtained from a stretched exponential fit.[39] [p] At 20 °C using coumarin 153.[36] [q] At 20 °C using Prodan.[36] [r] At 20 °C using 4-AP.[36] [s] At 298 K using Prodan.[53]

construct the time-resolved emission spectra were typically collected over a range of wavelengths from 470 to 610 nm at intervals of 10 nm; unless otherwise indicated, a total of 15 transients were used to construct the time-resolved emission spectra, from which the $C(t)$ values were obtained.

**Transient-Absorption (Stimulated-Emission) Measurements.** The instrument function of our time-correlated single-photon counting system has a fwhm of 80 ps. To investigate more rapid phenomena, better time resolution was required. This was provided by a homemade regeneratively amplified Ti−sapphire system,[44,45] providing 130-fs pulses, which we used to perform pump−probe transient stimulated-emission measurements. Samples were excited at 407 nm. ($[BMIM^+][Cl^-]$ was not investigated with this system because our rotating sample holder is not temperature controlled and because the solvent slowly solidifies at room temperature.)

The use of stimulated emission to measure solvation requires special conditions, notably that excited-state (and ground-state) absorption does not contaminate the signal. Such a situation should not be assumed to be the norm. Ernsting and co-workers[46] have studied the time-dependent spectra of coumarin 153. Their results suggested that the spectral regions near 480 and 560 nm are free of absorbing species. This was fortuitous because Gardecki and Maroncelli[47] indicated that 480 and 560 nm could be used for coumarin 153 to construct single-wavelength solvation correlation functions. Such a situation seemed to be optimal experimentally since laboratories are more typically equipped to perform transient absorption than fluorescence-upconversion experiments and because a single-wavelength analysis is obviously not as time-consuming as one requiring data collection over a range of wavelengths. Several research groups have discussed and employed the single-wavelength solvent-correlation function, $C_{SW}(t)$.[47−49] As a result, we measured stimulated-emission kinetics at 480 and 560 nm and typically collected over a full scale of 100 ps.

To have a picture of the solvation over the entire time scale, starting from "time zero" (as defined by the 130-fs pulses of the transient-absorption apparatus) to about 4 ns, the longest time scale we investigated with our photon-counting system, we spliced the data from the two experiments together and constructed the single-wavelength solvation response function at the probe wavelength of 480 nm. The decay curves from the stimulated emission and the photon-counting measurements were first fit to multiexponential functions. The data points for the first 100 ps were taken from the fitted stimulated-emission kinetics and from 100 ps to 4 ns, from the fitted photon-counting experiments. The spliced curves were normalized according to the following equation[47]

$$F'(\nu,t) = F(\nu,t)\, \exp\{+K_{tot}^{\infty} t\} \tag{4}$$

where $F(\nu,t)$ is the spliced emission curve and $\exp\{+K_{tot}^{\infty} t\}$ is the population factor. For our normalization, we used the inverse of the average fluorescence lifetime ($1/\langle\tau_F\rangle$), obtained from measuring the fluorescence decay while collecting light from most of the emission band, to approximate $K_{tot}$. An average lifetime is employed since the fluorescence decay is not well described by a single exponential. Once the population factor was taken into account, the normalized single-wavelength solvation-response curve, $C_{SW}(t)$, was constructed

$$C_{SW}(t) = \frac{F'(\nu_{SW},t) - F'(\nu_{SW},\infty)}{F'(\nu_{SW},0) - F'(\nu_{SW},\infty)} \tag{5}$$

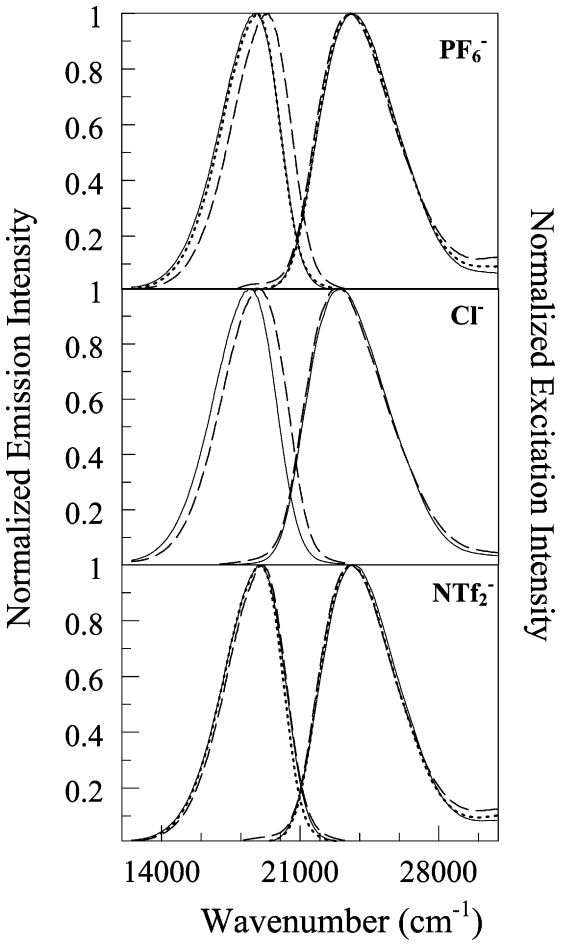


**Figure 2.** Excitation and emission spectra of coumarin 153 in [BMIM$^+$][$PF_6^-$] at 90 °C (solid) $\lambda = 2662$ cm$^{-1}$, 25 °C (dotted) $\lambda = 2592$ cm$^{-1}$, and −10 °C supercooled (dashed) $\lambda = 2272$ cm$^{-1}$; [BMIM$^+$][$Cl^-$] at 70 °C (solid) $\lambda = 2582$ cm$^{-1}$ and 30 °C supercooled (dashed) $\lambda = 2294$ cm$^{-1}$; [BMIM$^+$][$NTf_2^-$] at 90 °C (solid) $\lambda = 2649$ cm$^{-1}$, 25 °C (dotted) $\lambda = 2607$ cm$^{-1}$, and −10 °C supercooled (dashed) $\lambda = 2466$ cm$^{-1}$. All samples were excited at 420 nm. For excitation spectra, the emission monochromator was at 600 nm.

**Fluorescence-Upconversion Measurements.** The system used for these measurement is that of the amplified Ti−sapphire referred to above for the stimulated-emission experiments. The fundamental output from the amplifier (815 nm) is doubled by a type-I LBO crystal (2 mm). The frequency-doubled blue pulses (407 nm) are separated from the fundamental by a dielectric mirror coated for 400 nm and are focused onto a rotating cell containing the sample using a 5-cm convex lens. The remaining fundamental was used as the gate to upconvert emission. Fluorescence was collected by an LMH-10x microscopic objective (OFR Precision Optical Products) coated for near UV transmission. The gate and the emission are focused by a quartz lens (12 cm) onto a type-I 0.4-mm BBO crystal ($MgF_2$ coated, cut at 31°, and mounted by Quantum Technology, Inc). The polarization of both the gate and excitation source was controlled with a set of zero-order half-wave plates for 800 and 400 nm, respectively. The upconverted signal is then directed into an H10 (8 nm/mm) monochromator (Jobin Yvon/Spex Instruments S. A. Group) with a 5-cm convex lens coupled to a Hamamatsu R 980 PMT equipped with a UG11 UV-pass filter and operated at maximum sensitivity. The PMT output was amplified in two stages (total by a factor of 25, 5 for each stage) by a Stanford research Systems SR-445 DC-300 MHz amplifier with input terminated at 500 Ω and was carefully calibrated after a long (1−2 h) warm-up. Photon arrival events were registered with

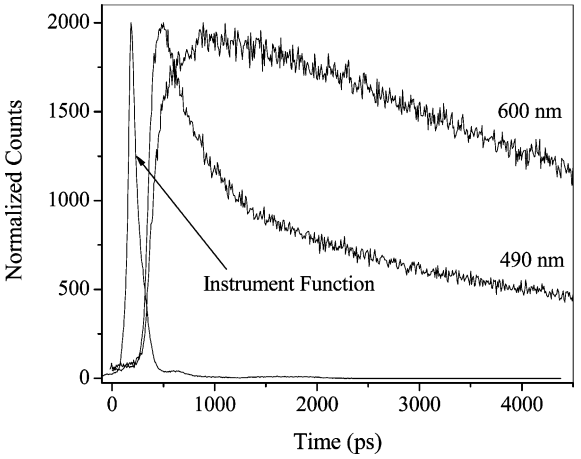


**Figure 3.** Representative wavelength-resolved decays for C153 [BMIM$^+$][$NTf_2^-$] at 490 and 600 nm. A typical instrument function profile is included. The trace at 600 nm reveals the growth of a solvent-relaxed state (which is absent in the profile at 490 nm). The decays used to construct the time-resolved emission spectra were typically collected over a range of wavelengths from 470 to 610 nm at intervals of 10 nm; a total of fifteen time-resolved fluorescence traces were used to construct the time-resolved emission spectra, from which the $C(t)$ values were obtained.

SR-400 gated photon counter operated in CW mode with a threshold level of −100 mV. This signal was fed into a boxcar averager. A part of the blue pulse train was used to normalize pump-beam fluctuations. A translation stage (Compumotor) with a resolution of 0.06 mm/step was used to delay the exciting pulses and a computer with an interfacing card from Keithley Metrabyte (DAS 800) was used for driving the motor. The instrument-response function was obtained by collecting the cross-correlation function of the blue and red pulses; the resulting third harmonic intensity was plotted against delay time. The cross-correlation functions typically have a fwhm of ∼1 ps. This instrument response is a little over 3 times as broad as that obtained with our unamplified system.[50,51] We attribute this to the absence of compensating prisms after frequency doubling, the presence of the rotating sample cell, and perhaps a nonideal optical geometry, which nevertheless permits the facile interchange between pump−probe transient absorption and fluorescence-upconversion measurements. All curves were fit and deconvoluted from the instrument function using an iterative convolute and compare least-squares algorithm.

## Results

Table 1 summarizes most of the results obtained in this study. (Upconversion results will be discussed separately.) Figure 2 presents excitation and emission spectra of coumarin 153 in the three ionic liquids for which we were able to obtain spectra above and below their melting points (while the ionic liquids still remained liquid). The significant feature is that the emission spectra of coumarin 153 are superimposable at all temperatures in a given solvent unless the spectra are obtained using the supercooled liquid.

Figure 3 presents two typical wavelength-resolved decay profiles of coumarin 153 in [BMIM$^+$][$NTf_2^-$]. Figure 4 gives the solvation correlation functions, $C_{SR}(t)$, constructed from the time-correlated single-photon counting data using the spectral reconstruction method.

The single-wavelength solvent-response functions, $C_{SW}(t)$, obtained at 480 nm from combining the stimulated-emission and the photon-counting results are shown in Figure 5. These results are direct measurements of the early rapid solvation

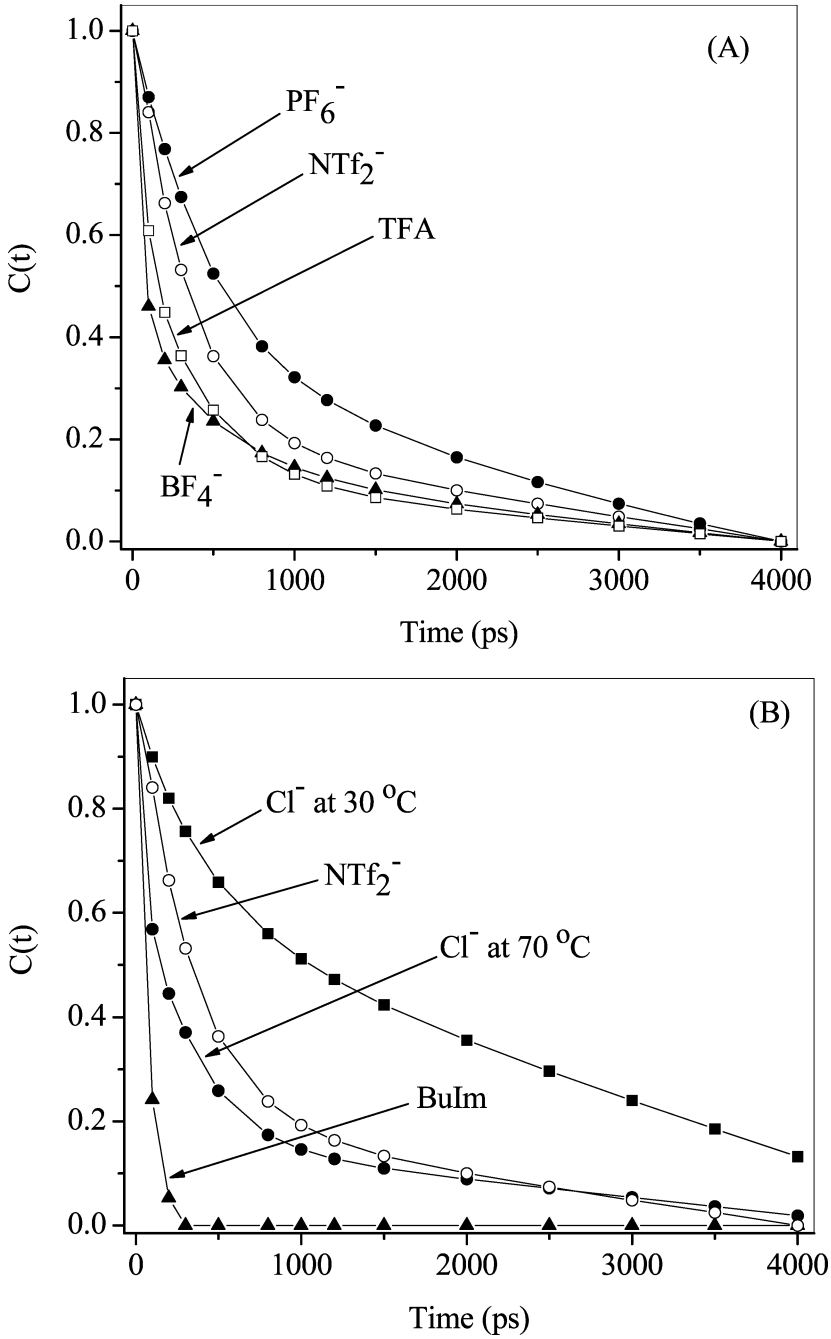


**Figure 4.** $C_{SR}(t)$ curves and corresponding fits for C153 in (A) [BMIM$^+$][NTf$_2^-$] (○) [$C(t)$ = 0.72 exp(−$t$/350 ps) + 0.28 exp(−$t$/1670 ps)]; [BMIM$^+$][PF$_6^-$] (●) [$C(t)$ = 0.36 exp(−$t$/360 ps) + 0.64 exp(−$t$/1360 ps)]; [BMIM$^+$][BF$_4^-$] (▲) [$C(t)$ = 0.62 exp(−$t$/60 ps) + 0.38 exp(−$t$/1100 ps)]; [NHEt$_3^+$][TFA$^-$] (□) [$C(t)$ = 0.58 exp(−$t$/120 ps) + 0.42 exp(−$t$/940 ps)] and (B) [BMIM$^+$][Cl$^-$] at 30 °C (■) [$C(t)$ = 0.24 exp(−$t$/270 ps) + 0.76 exp(−$t$/2530 ps)]; [BMIM$^+$][Cl$^-$] at 70 °C (●) [$C(t)$ = 0.63 exp(−$t$/120 ps) + 0.37 exp(−$t$/1290 ps)]; [BMIM$^+$][NTf$_2^-$] (○); butylimidazole (▲) [$C(t)$ = exp(−$t$/70 ps)].

process in these ionic liquids, at least 50% of which is completed in the first 100 ps. In general, this method reports a fast solvation component of 40−70 ps, which is considerably longer than the <5 ps suggested by Maroncelli and co-workers [37,39] based on their estimation of the resolution of their time-correlated single-photon counting apparatus. The significance and accuracy of our result will be discussed in more detail below.

A comparison of the solvation correlation functions obtained from the single-wavelength and the spectral-reconstruction methods is given in Figure 6 and in Table 1 in order to provide a check on the appropriateness of using the stimulated-emission data to measure the initial rapid phase of solvation. The agreement between the two methods is often quite good, as in the cases of [BMIM$^+$][Cl$^-$] at 70 °C, [BMIM$^+$][BF$_4^-$], and butylimidazole. It is rather poor in the cases of [BMIM$^+$][PF$_6^-$] and [BMIM$^+$][NTf$_2^-$] (not shown). The agreement in general appears poorer upon comparison of the average solvation times in Table 1 than when visually inspecting the form of the correlation functions. This is because the curves fail to superimpose in the long-time region, where even low-amplitude slow dynamics can contribute considerably to the average. Even in this long-time region, however, the form of the two correlation functions may remain similar, as can be seen by comparing the data for [BMIM$^+$][Cl$^-$] at 70 °C and [BMIM$^+$][BF$_4^-$].

Fluorescence-upconversion measurements provide an independent gauge of the time scale for this initial rapid process.

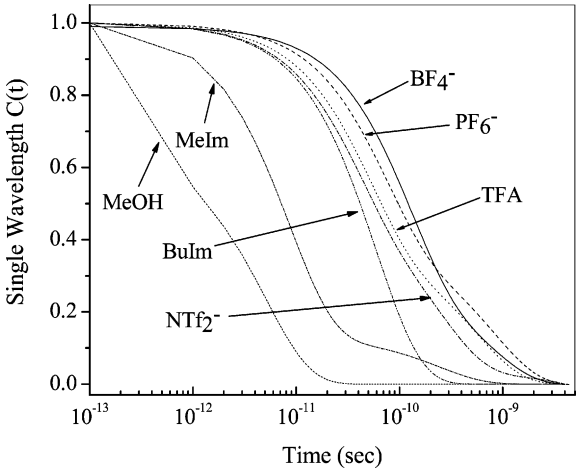


**Figure 5.** $C_{SW}(t)$ for C153 obtained at 480 nm at room temperature. The plots are stimulated-emission kinetics obtained over 100 ps with 130-fs pulses and, where necessary, time-correlated single-photon counting data obtained over 4 ns with an 80-ps instrument function. The two traces were spliced together at 100 ps in order to present a continuous trace of the solvation dynamics. Global fits to the $C_{SW}(t)$ are summarized in Table 2. The $C_{SW}(t)$ for methanol is presented as a "control" experiment, yielding an average solvation time of 3.5 ps. That the fast solvation components of the $BMIM^+$ liquids resemble that of butylimidazole and that the fast component is seen to become more rapid as the solvent is changed to methylimidazole or to methanol suggests that the ~55-ps event in the ionic liquids is a plausible result. See, however, the correlation functions obtained from fluorescence-upconversion data in Figures 7, 8, and 10.

Whereas stimulated-emission (i.e., transient-absorption) measurements are sensitive to both emitting and absorbing species, fluorescence measurements report only on spontaneous emission and thus provide a more straightforward means of probing the solvation behavior of interest. Upconversion data are provided in Figures 7−9 for $[BMIM^+][PF_6^-]$, butylimidazole, and methanol. For each of the solvents, the transients obtained using the two methods are compared at 480 and 560 nm, the wavelengths suggested for use in single-wavelength analysis for coumarin 153.[47] For each solvent, there are deviations arising from excited-state absorbance at these wavelengths, which conspire to distort the time scale for solvation.

## Discussion

**Steady-State Spectra.** Steady-state spectra taken as a function of temperature are presented in Figure 2 for three RTILs. Spectra obtained at temperatures above the melting point are nearly superimposable. These three solvents can be supercooled easily. Once the temperature is lowered below the melting point, crystallization occurs slowly. In the case of $[BMIM^+][Cl^-]$, it can occur over a period of several days. Upon supercooling, a significant change in the spectra is observed, which is manifest essentially in their position. There is less solvent relaxation, which we have quantified by means of the reorganization energy, $\lambda$ (Table 1 and Figure 2). In the case of $[BMIM^+][Cl^-]$, $\lambda$ decreases from 2582 $cm^{-1}$ at 70 °C to 2294 $cm^{-1}$ for the supercooled liquid at 30 °C. This shift suggests that the solvent is essentially "glassy" in the supercooled state. For $[BMIM^+][Cl^-]$, supercooling increases the average solvation time by about a

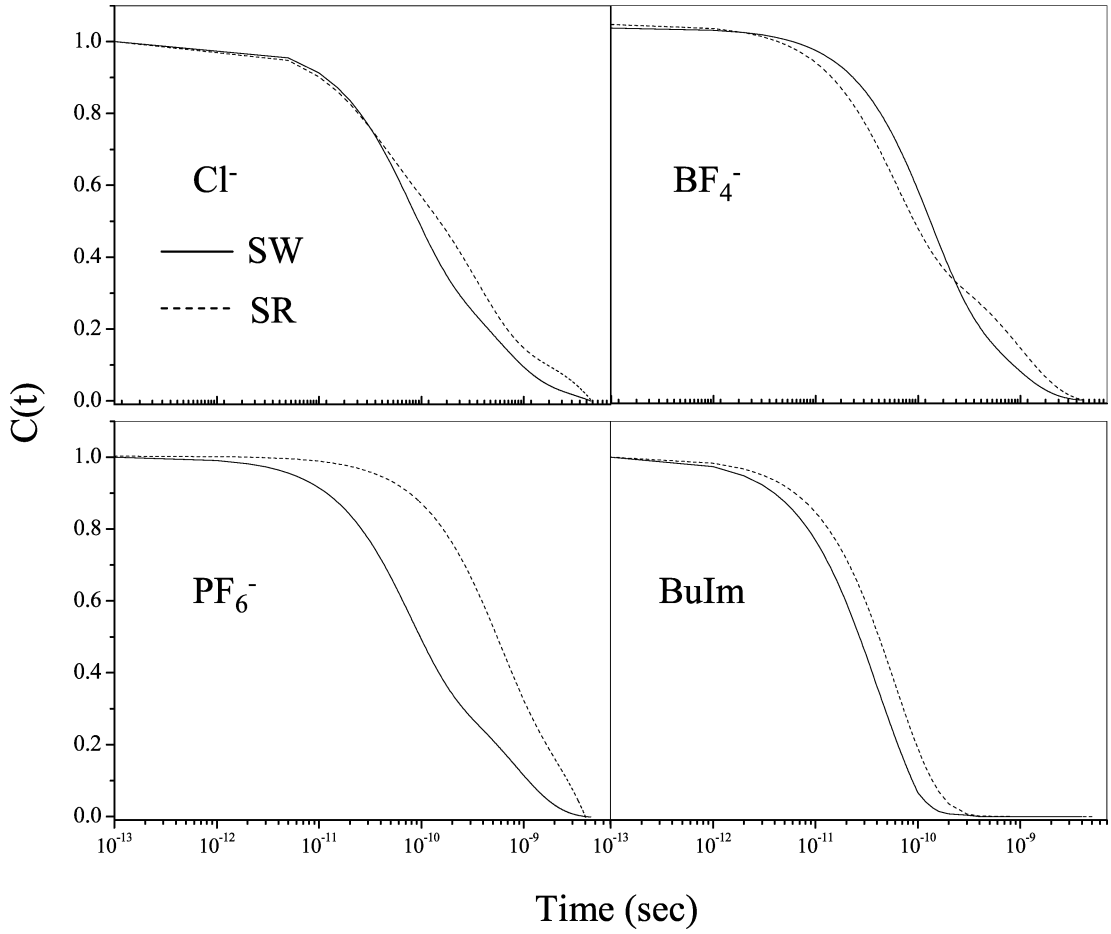


**Figure 6.** A comparison of the solvation correlation functions obtained from the single-wavelength (solid lines), $C_{SW}^{480nm}(t)$, and the spectral-reconstruction (dashed lines), $C_{SR}(t)$, methods. All data were obtained from time-correlated single-photon counting experiments. A complete comparison is given in Tables 1 and 2. The agreement ranges from very good for $[BMIM^+][Cl^-]$ at 70 °C and $[BMIM^+][BF_4^-]$ to poor for $[BMIM^+][PF_6^-]$.

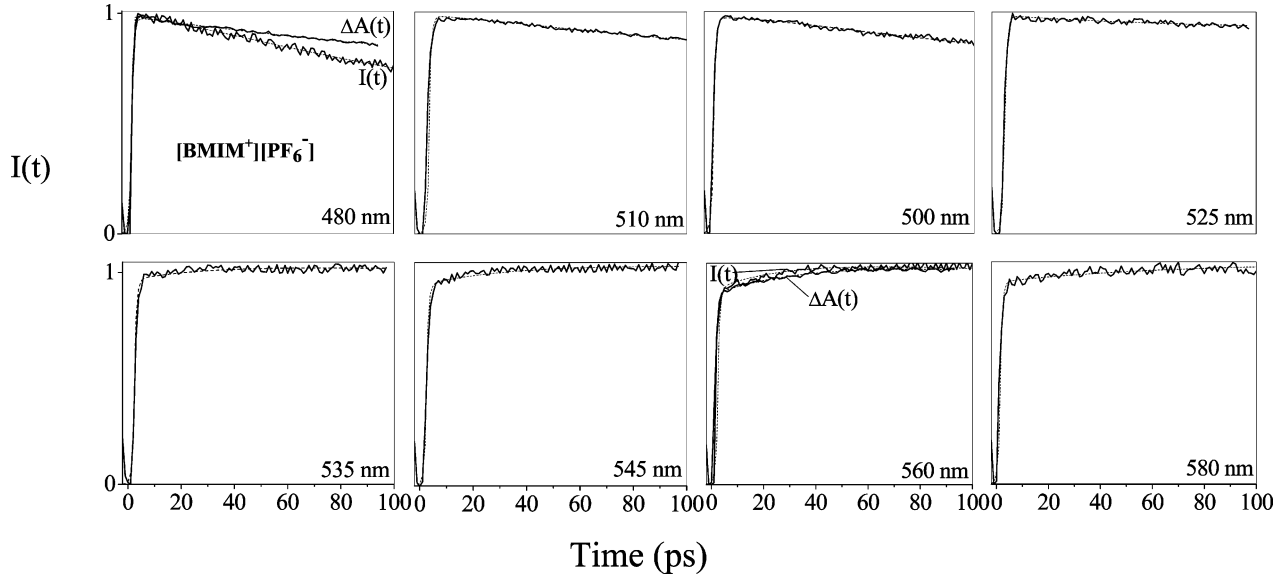


**Figure 7.** Normalized upconversion traces, $I(t)$, for C153 in $[BMIM^+][PF_6^-]$ at different wavelengths. $\Delta A(t)$ is the kinetic trace for the pump−probe stimulated-emission experiment at the corresponding wavelength. All upconversion traces are fitted globally with time constants of 5, 210, and 5100 ps.

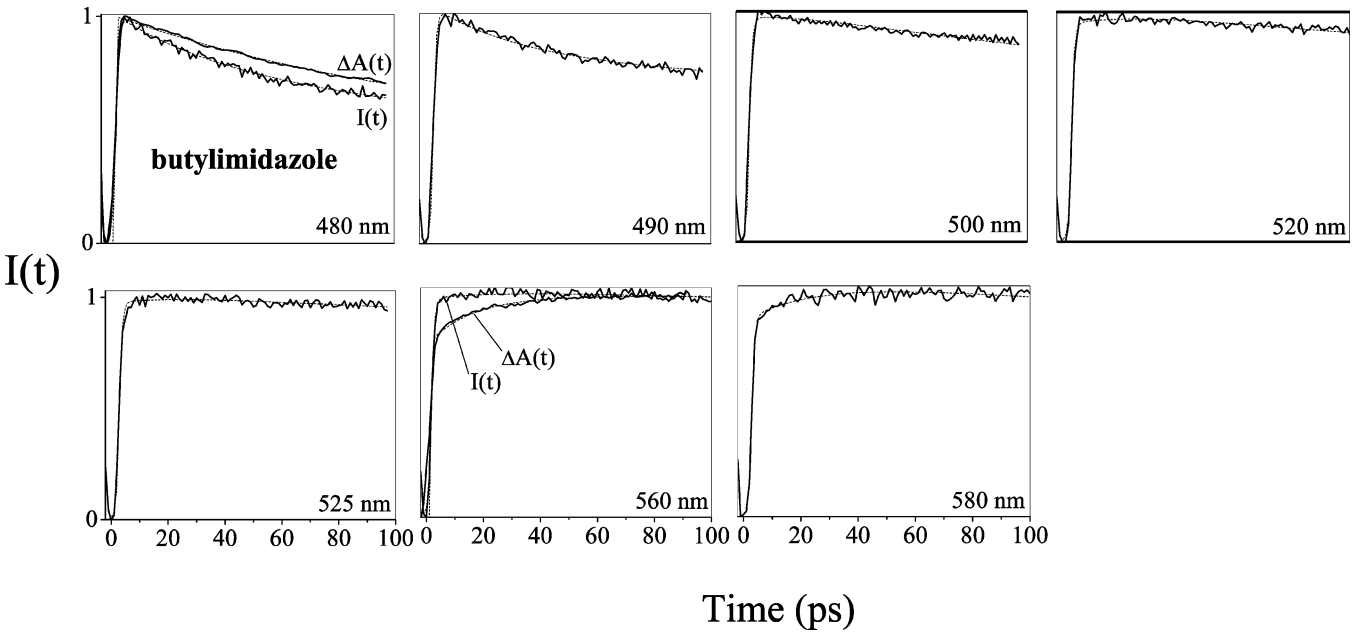


**Figure 8.** Normalized upconversion traces, $I(t)$, for C153 in butylimidazole at different wavelengths. $\Delta A(t)$ is the kinetic trace for the pump−probe stimulated-emission experiment at the corresponding wavelength. All upconversion traces are fitted globally with the following time constants: 28, 102, and 4700 ps.

factor of 4. An interesting aspect of the spectra is that the change in reorganization energy between the normal (90 °C) and the supercooled liquids (−10 °C) is much smaller for $[BMIM^+][NTf_2^-]$ than for $[BMIM^+][Cl^-]$ and $[BMIM^+][PF_6^-]$: $\Delta\lambda = 183$, 288, and 390 $cm^{-1}$, respectively (see the caption to Figure 2). That the change is the smallest for $[BMIM^+][NTf_2^-]$ may be attributed to it having the lowest viscosity of the three solvents; upon supercooling, it is immobilized to a lesser degree than $[BMIM^+][Cl^-]$ or $[BMIM^+][PF_6^-]$. We were unable to perform the same temperature-dependent analysis with the $BF_4^-$ solvent because it melts at −82 °C and our apparatus did not permit us to obtain such a temperature. Maroncelli and co-workers[37,39] have recently shown that ionic liquids conform to standard glass behavior by fitting their kinetic data to stretched exponentials and by showing that it varies linearly with viscosity.

**Stimulated-Emission, Time-Correlated Single-Photon Counting, and Single-Wavelength Analysis.** Inspection of Table 1 indicates that there is a considerable disparity in the values of the average solvation times obtained from different laboratories using the spectral reconstruction method. Reasonable agreement is obtained between our result for $[BMIM^+][PF_6^-]$ and those results of Maroncelli and co-workers using 4-AP and coumarin 102.[37] There is also reasonable agreement between our result for $[BMIM^+][NTf_2^-]$ and those of Karmakar and Samanta using coumarin 153 and Prodan.[36] Some of the disparity may be attributed to the number of counts collected in the fluorescence decay, which affects the signal-to-noise ratio, and to the full-scale time window used, which determines how accurately the long-time component is determined. In our case, we use ∼4 ns, which is smaller than that used by other groups.

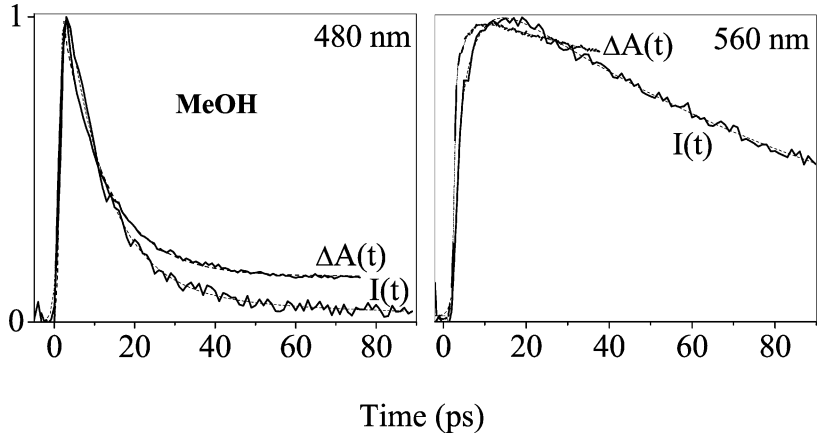


**Figure 9.** Normalized upconversion traces, $I(t)$, for C153 in MeOH at 480 and 560 nm along with the stimulated-emission traces, $\Delta A(t)$, obtained at the same wavelengths.

A more significant origin of the discrepancies may arise from the preparation and purity of the ionic liquids themselves. Trace amounts of water and chloride impurities are known to have large effects on the viscosities and densities of RTILs.[52] Notably, Bright and co-workers[53] report that the average solvation time of Prodan in $[BMIM^+][PF_6^-]$ decreases from 6.5 to 3.9 ns as the water content is increased from <50 ppm to 1.8 wt %. Since the focus of this article is not to obtain a *quantitative* comparison of the long-time behavior of the RTILs, these differences do not cause excessive concern. They should, however, give an indication to future workers of the spectrum of results that have been obtained with an eye to ensuring reproducibility when examining the glassiness of the RTILs.

Of more immediate interest in this work is the initial rapid phase of solvation in the ionic liquids. Several previous studies[34−39] have suggested, and our results indicate (Figures 4 and 5), that more than 50% of solvation relaxation is very rapid. The origin of these fast solvent fluctuations is not clear. We have hypothesized that the fast relaxations result from the organic cations. To test this idea, we attempted to compare the solvation dynamics of butylimidazole with those of the four ionic liquids bearing the BMIM cation. A comparison of $[NHEt_3^+][TFA^-]$ with triethylamine was, unfortunately, not possible because triethylamine quenches excited-state coumarin by electron transfer.[54] We attempted other comparisons with RTILs formed from butylpyridinium and pyridinium organic cations with $BF_4^-$ and $NTf_2^-$. These also presented complications in the excited-state kinetics that prevented a further comparison of solvation dynamics of the RTILs with their organic counterparts.

The organic solvent, butylimidazole, has a solvation time of between 40 and 70 ps (Figures 4 and 5, Tables 1 and 2). Butylimidazole has a very low viscosity, and amplitudes of the fast components of the solvation times for the ionic liquid counterparts seem to scale with viscosity, as indicated by Figure 5 and Table 2. The latter presents the results of a global fitting analysis to the $C_{SW}(t)$ functions (except where indicated). In this procedure, the $C_{SW}(t)$ were fit to two decaying exponential components where the smallest time constant was fixed to agree roughly with that of butylimidazole, 55 ps. The amplitudes of the two components and the time constant of the longer were permitted to vary. A 55-ps component was present in all the fits. Such a value seems reasonable given that the time constant and the average solvation time for butanol, obtained by fluorescence measurements, are 47 and 63 ps, respectively.[55] Another point of comparison is provided by the $C_{SW}(t)$ of methylimidazole (Figure 5 and Table 2), which is dominated by a rapid component of 8.5 ps. The time constant and average solvation time for methanol, as measured by fluorescence techniques, are 2.3 and 5.0 ps, respectively.[55] Our $C_{SW}(t)$ for coumarin 153 in methanol (Figure 5) obtained from stimulated-emission kinetics is described by an average solvation time of 3.5 ps. This suggests that ionic liquids based on the methylimidazolium cation will have much faster initial solvation components owing to the shortening of the aliphatic chain from butyl to methyl, just as the solvation by the alcohols is faster for methanol than for butanol. A more direct test of this hypothesis will require measurements of the solvation times of different RTILs at the same viscosity as well as a comparison with ionic liquids based on other cations.

**TABLE 2: Global Fitting of the Initial Rapid Phase of $C_{SW}(t)$ of Some RTILs[a]**

| ionic liquid | $\eta$ (cP)[b] | $a_1$ | $\tau_1$ (ps) | $\tau_2$ (ps) |
|---|---|---|---|---|
| $[BMIM^+][BF_4^-]$ (20 °C) | 154[52] 233[57] | 0.39 | 55 | 1000 |
| $[NHEt_3^+][TFA^-]$ (20 °C) | | 0.61 | 55 | 650 |
| $[BMIM^+][PF_6^-]$ (20 °C) | 371[52] 312[57] | 0.62 | 55 | 2250 |
| $[BMIM^+][NTf_2^-]$ (20 °C) | 52[57] | 0.73 | 55 | 1500 |
| butylimidazole (20 °C) | < 50 | 0.98 | 55 | 120 |
| methylimidazole (20 °C) | < 50 | 0.80 | 8.5 | 190 |
| methanol (20 °C) | 0.59 | 0.35 | 0.32 | 5.2 |

[a] $C_{sw}(t)$ obtained from 480-nm stimulated-emission data as described in the text are fit to a sum of exponentials, $C_{sw}(t) = a_1 \exp(-t/\tau_1) + a_2 \exp(-t/\tau_2)$, where $a_1 + a_2 = 1$. In all cases (except the last two solvents), the rapid-solvation component is fixed at 55 ps. Given the 100-ps full scale used in most cases (for $[NHEt_3^+][TFA^-]$, a 400-ps scale was used), the longer-lived components should not be regarded as accurate estimations of the slower solvation phase. The $C_{sw}(t)$ are displayed in Figure 5. [b] We have no viscosity information for $[NHEt_3^+][TFA^-]$ and have not been able to obtain any for butylimidazole or methylimidazole from either the literature or the supplier.

On the other hand, another interpretation of the origin of the initial fast component has resulted from a recent computer simulation. Shim et al.[40] place a dipolar excitation on a model diatomic solute in a RTIL. They observe fast initial relaxation apparently arising from translations of the anions. Given the small size of the model solute and the large changes in net charge, the motions of the resulting concentrated anionic charges may dominate the relaxation. In the experimental solvation dynamics studies of organic dye molecules such as coumarin 153 in RTILs, the charge distribution change is scattered across the whole probe molecule, which is most likely well solvated by the cations given the hydrophobic nature of C153 in the ground state. We suggest, therefore, that the most possible

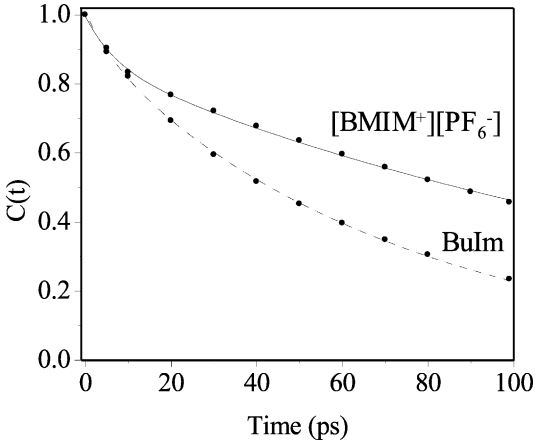


**Figure 10.** Solvation correlation functions, $C_{SR}(t)$, for $[BMIM^+][PF_6^-]$ (solid line) and butylimidazole (dashed line). The correlation functions are well described by the following forms: $[BMIM^+][PF_6^-]$, 0.14 exp($-t$/7 ps) + 0.86 exp($-t$/160 ps); butylimidazole, 0.09 exp($-t$/7 ps) + 0.91 exp($-t$/72 ps). It is likely that the relative amplitude of the short component in these correlation functions is reduced with respect to those obtained from stimulated-emission measurements owing to the poorer time resolution of ~1 ps.

scenario is that the cation motions dominate the contribution of the initial fast relaxation upon excitation. To elucidate the nature of the fast relaxations, a realistic model of C153 in RTILs will be needed. Znamenskiy and Kobrak have recently performed molecular dynamics simulations of the dye betaine-30 in $[BMIM^+][PF_6^-]$.[56] They obtain radial distribution functions indicating the proximity of the 1-butyl-3-methylimidazolium ring to the dye, which is consistent with our experimental observations for coumarin.

**Analysis Based upon Fluorescence-Upconversion Results.** Finally, we wish to comment on the relative merits of using stimulated-emission measurements, single-wavelength construction of $C(t)$, and direct fluorescence measurements. The comparison provided here, in particular the data presented in Figures 6−9, indicate that while the stimulated-emission measurements provide a good qualitative picture of the dynamics, they deviate considerably from the fluorescence-upconversion measurements. We have already noted the discrepancies in the sub-nanosecond and nanosecond time regimes using single-wavelength and "complete" spectral data from photon-counting measurements (Figure 6). The fluorescence-upconversion measurements permit us to make this comparison in the picosecond time regime. Examination of the traces at 480 and 560 nm indicates that there is at least one absorbing species that contributes to the stimulated-emission signal. In the absence of absorption, the two techniques should give identical results. But in fact, for $[BMIM^+][PF_6^-]$ and butylimidazole, excited-state absorption causes the stimulated-emission kinetics at 480 and 560 nm to decay and rise, respectively, slower than those of their spontaneous-emission counterparts. This translates into an overestimation of the time scale for solvation by a factor of ~8. Deviations are also apparent for methanol. In particular, while the fluorescence-upconversion trace in methanol decays essentially to zero, the stimulated-emission trace levels off at about 40 ps to a steady-state value of about 20% of the initial signal intensity, again indicating the presence of one or more absorbing states.

Figure 10 presents the $C_{SR}(t)$ for $[BMIM^+][PF_6^-]$ and butylimidazole obtained from the data in Figures 7 and 8, respectively. These solvation correlation functions can both be fit to the same initial rapid component of 7 ps, and as such, the role of the organic cation suggested by the stimulated-emission studies is corroborated. A more comprehensive comparison is, however, required and is currently being undertaken.

## Conclusions

Our results are generally consistent with those of previous workers,[34−39] but there are significant discrepancies in the average solvation times reported for some ionic liquids, most likely arising from the determination of the longer-lived dynamics. Solvation times obtained from the spectral-resolution and the single-wavelength methods are compared. Our stimulated-emission experiments with sub-picosecond time resolution are the first to probe directly the initial rapid solvation component that had been suggested in the earlier studies. They yield a time constant in the range of 40−70 ps (Figure 5, Table 2). Nevertheless, fluorescence-upconversion measurements indicate that the presence of excited-state absorption increases this time by approximately a factor of 8 from its value as obtained by monitoring spontaneous emission directly. Consequently, while stimulated-emission measurements can be useful in indicating general trends, direct measurements of spontaneous emission and use of spectral reconstruction methods are required for quantitative work. These results lead one to inquire into the nature and the number of the excited states contributing to this absorption since their presence could profoundly affect the interpretation of solvation dynamics data. Finally, a comparison of the solvation times in the 1-butyl-3-methylimidazolium ionic liquids with that of butylimidazole itself (and methylimidazole) leads us to consider the role of the polarizability of the cationic partner in giving rise to the initial rapid solvation component.

**Acknowledgment.** D.W.A. was supported by NIH Grant RO1 GM53825-08. We thank Dr. Ranjan Das for technical assistance in collecting the fluorescence-upconversion data. Edward Castner and Mark Maroncelli provided stimulating comments. We thank the latter for sharing his Kerr-gated fluorescence data with us before publication.

## References and Notes

(1) Seddon, K. R. *Nature (Materials)* **2003**, *2*, 363.
(2) Anderson, J. L.; Ding, J.; Welton, T.; Armstrong, D. W. *J. Am. Chem. Soc* **2002**, *124*, 14247.
(3) Wilkes, J. S.; Zaworotko, M. J. *J. Chem. Soc., Chem. Commun.* **1992**, 965.
(4) Adams, C. J.; Earle, M. J.; Roberts, G.; Seddon, K. R. *Chem. Commun.* **1998**, 2097.
(5) Earle, M. J.; McCormac, P. B.; Seddon, K. R. *Chem. Commun. (Cambridge)* **1998**, 2245.
(6) Dyson, P. J.; Ellis, D. J.; Parker, D. G.; Welton, T. *Chem. Commun. (Cambridge)* **1999**, 25.
(7) Leadbeater, N. E.; Torenius, H. M. *J. Org. Chem.* **2002**, *67*, 3145.
(8) Mann, B. E.; Guzman, M. H. *Inorg. Chim. Acta* **2002**, *330*, 143.
(9) Wasserscheid, P.; Keim, W. *Angew. Chem., Int. Ed.* **2000**, *39*, 3772.
(10) Reynolds, J. L.; Erdner, K. R.; Jones, P. B. *Org. Lett.* **2002**, *4*, 917.
(11) Welton, T. *Chem. Rev.* **1999**, *99*, 2071.
(12) Nara, S. J.; Harjani, J. R.; Salunkhe, M. M. *Tetrahedron Lett.* **2002**, *43*, 2979.
(13) Yao, Q. *Org. Lett.* **2002**, *4*, 2197.
(14) Fletcher, K. A.; Pandey, S.; Storey, I. K.; Hendricks, A. E.; Pandey, S. *Anal. Chim. Acta* **2002**, *453*, 89.
(15) Grodkowski, J.; Neta, P. *J. Phys. Chem. A* **2002**, *106*, 5468.
(16) Handy, S. T.; Zhang, X. *Org. Lett.* **2001**, *3*, 233.
(17) Huddleston, J. G.; Rogers, R. D. *Chem. Commun.* **1998**, 1765.
(18) Dai, S.; Ju, Y. H.; Barnes, C. E. *J. Chem. Soc., Dalton Trans.* **1999**, 1201.
(19) Dickinson, V. E.; Williams, M. E.; Hendrickson, S. M.; Masui, H.; Murray, R. W. *J. Am. Chem. Soc.* **1999**, *121*, 613.
(20) Armstrong, D. W.; Zhang, L.-K.; He, L.; Gross, M. L. *Anal. Chem.* **2001**, *73*, 3679.
(21) Muldoon, M. J.; Gordon, C. M.; Dunkin, I. R. *J. Chem. Soc., Perkin Trans. 2* **2001**, 433.

(22) Carmichael, A. J.; Seddon, K. R. *J. Phys. Org. Chem.* **2000**, *13*, 591.
(23) Bonhote, P.; Dias, A.-P.; Papageorgiou, N.; Kalyanasundaram, K.; Graetzel, M. *Inorg. Chem.* **1996**, *35*, 1168.
(24) Aki, S. N. V. K.; Brennecke, J. F.; Samanta, A. *Chem. Commun (Cambridge)* **2001**, 413.
(25) Armstrong, D. W.; He, L.; Liu, Y.-S. *Anal. Chem.* **1999**, *71*, 3873.
(26) Abraham, M. H.; Whiting, G. S.; Doherty, R. M.; Shuely, W. J. *J. Chromatogr., A* **1990**, *518*, 329.
(27) Abraham, M. H.; Whiting, G. S.; Andonian-Haftvan, J.; Steed, J. W. *J. Chromatogr., A* **1991**, *588*, 361.
(28) Abraham, M. H.; Whiting, G. S.; Doherty, R. M.; Shuely, W. J. *J. Chromatogr., A* **1991**, *587*, 213.
(29) Maroncelli, M.; Fleming, G. R. *J. Chem. Phys.* **1987**, *86*, 6221.
(30) Vajda, S.; Jimenez, R.; Rosenthal, S. J.; Fidler, V.; Fleming, G. R.; Castner, E. W. *J. Chem. Soc., Faraday Trans.* **1995**, *91*, 867.
(31) Huppert, D.; Ittah, V.; Kosower, E. M. *Chem. Phys. Lett.* **1989**, *159*, 267.
(32) Ittah, V.; Huppert, D. *Chem. Phys. Lett.* **1990**, *173*, 496.
(33) Chapman, C. F.; Maroncelli, M. *J. Phys. Chem.* **1991**, *95*, 9095.
(34) Karmakar, R.; Samanta, A. *J. Phys. Chem. A* **2002**, *106*, 4447.
(35) Karmakar, R.; Samanta, A. *J. Phys. Chem. A* **2002**, *106*, 6670.
(36) Karmakar, B.; Samanta, A. *J. Phys. Chem. A* **2003**, *107*, 7340.
(37) Ingram, J. A.; Moog, R. S.; Ito, N.; Biswas, R.; Maroncelli, M. *J. Phys. Chem. B* **2003**, *107*, 5926.
(38) Chakrabarty, D.; Hazra, P.; Chakraborty, A.; Seth, D.; Sarkar, N. *Chem. Phys. Lett.* **2003**, *381*, 697.
(39) Arzhantsev, S.; Ito, N.; Heitz, M.; Maroncelli, M. *Chem. Phys. Lett.* **2003**, *381*, 278.
(40) Shim, Y.; Duan, J.; Choi, M. Y.; Kim, H. J. *J. Chem. Phys.* **2003**, *119*, 6411.
(41) Hyun, B.-R.; Dzyuba, S. V.; Bartsch, R. A.; Quitevis, E. L. *J. Phys. Chem. A* **2002**, *106*, 7579.
(42) Giraud, G.; Gordon, C. M.; Dunkin, I. R.; Wynne, K. *J. Chem. Phys.* **2003**, *119*, 464.
(43) Jordanides, X. J.; Lang, M. J.; Song, X. Y.; Fleming, G. R. *J. Phys. Chem. B* **1999**, *103*, 7995.
(44) English, D. S.; Zhang, W.; Kraus, G. A.; Petrich, J. W. *J. Am. Chem. Soc.* **1997**, *119*, 2980.
(45) English, D. S.; Das, K.; Zenner, J. M.; Zhang, W.; Kraus, G. A.; Larock, R. C.; Petrich, J. W. *J. Phys. Chem. A* **1997**, *101*, 3235.
(46) Kovalenko, S. A.; Ruthmann, J.; Ernsting, N. P. *Chem. Phys. Lett.* **1997**, *271*, 40.
(47) Gardecki, J. A.; Maroncelli, M. *J. Phys. Chem. A* **1999**, *103*, 1187.
(48) Nagarajan, V.; Brearley, A. M.; Kang, T.-J.; Barbara, P. F. *J. Chem. Phys.* **1987**, *86*, 3183.
(49) Changenet-Barret, P.; Choma, C. T.; Gooding, E. F.; DeGrado, W. F.; Hochstrasser, R. M. *J. Phys. Chem. B* **2000**, *104*, 9322.
(50) Das, K.; Smirnov, A. V.; Wen, J.; Miskovsky, P.; Petrich, J. W. *Photochem. Photobiol.* **1999**, *69*, 633.
(51) Smirnov, A. V.; Das, K.; English, D. S.; Wan, Z.; Kraus, G. A.; Petrich, J. W. *J. Phys. Chem. A* **1999**, *103*, 7949.
(52) Seddon, K. R.; Stark, A.; Torres, M.-J. Viscosity and Density of 1-Alkyl-3-methylimidazolium Ionic Liquids. In *Clean Solvents: Alternative Media for Chemical Reactions and Processing*; ACS Symposium Series; American Chemical Society, Washington, DC, 2002; Vol. 819, p 34.
(53) Baker, S. N.; Baker, G. A.; Munson, C. A.; Chen, F.; Bukowski, E. J.; Cartwright, A. N.; Bright, F. V. *Ind. Eng. Chem. Res.* **2003**, *42*, 6457.
(54) Castner, E. W., Jr.; Kennedy, D.; Cave, R. J. *J. Phys. Chem. A* **2000**, *104*, 2869.
(55) Horng, M. L.; Gardecki, J.; Papazyan, A.; Maroncelli, M. *J. Phys. Chem.* **1995**, *99*, 17311.
(56) Znamenskiy, V.; Kobrak, M. N. *J. Phys. Chem. B* **2004**, *108*, 1072.
(57) Carda-Broch, S.; Berthod, A.; Armstrong, D. W. *Anal. Bioanal. Chem.* **2003**, *375*, 191.
(58) Fee, R. S.; Maroncelli, M. *Chem. Phys.* **1994**, *183*, 235.